APPROXIMATING NON-LINEAR INDUCTORS USING TIME-VARIANT LINEAR FILTERS

Giulio Moro
Centre for Digital Music
Queen Mary University of London
London, United Kingdom
g.moro@qmul.ac.uk

Andrew P. McPherson
Centre for Digital Music
Queen Mary University of London
London, United Kingdom
a.mcpherson@qmul.ac.uk

ABSTRACT

In this paper we present an approach to modeling the non-linearities of analog electronic components using time-variant digital linear filters. The filter coefficients are computed at every sample depending on the current state of the system. With this technique we are able to accurately model an analog filter including a non-linear inductor with a saturating core. The value of the magnetic permeability of a magnetic core changes according to its magnetic flux and this, in turn, affects the inductance value. The cutoff frequency of the filter can thus be seen as if it is being modulated by the magnetic flux of the core. In comparison to a reference non-linear model, the proposed approach has a lower computational cost while providing a reasonably small error.

1. INTRODUCTION

This work investigates how it is possible to use linear, time variant filters in order to introduce non-linearities in a digital signal processing system. The idea is to use time-varying infinite impulse response filters whose coefficients are updated at every time sample according to the state of the system at the previous time sample. This approach is applied here to solve electronic circuits with non-linear components in the digital domain and can be used as a building block for Virtual Analog applications.

Non-linear DSP systems are governed by non-linear equations that have to be solved iteratively at a non-negligible computational cost [1, 2]. Adding a new non-linear equation to an existing system increases the computational cost even further and requires sometimes to partially re-design the existing system [3]. Non-iterative ways to solve such systems have been proposed which rely on pre-computed tables [4]. The lookup tables method does not scale up easily to systems with multiple non-linearities as this increases the dimensionality of the table, increasing memory usage and computational cost.

The method presented in this paper replaces the non-linear equations with a time-varying linear filter, which is by itself less expensive in terms of computations and can, potentially, be expanded to replace systems with multiple non-linearities with higher-order filters. We do not expect the output of our approximated model to be a sample-by-sample replica of the results obtainable with more accurate simulations, but we expect it to be close enough that the loss in accuracy is justified by improvements in execution speed and scalability.

While general criteria that determine the stability of stationary recursive filters are well defined in the literature [5], criteria to assess the stability of time-variant linear filters can be studied and defined only under some specific conditions. Existing work mainly focuses on bounded input-bounded output stability [6, 7] and transient suppression [8]. However, these methods are not readily applicable when filter coefficients are changing at every sample. Recent work proves that stable time-varying behavior can be obtained using state variable filters [9]. However, as in this paper we deal with passive first-order filters, we chose to use a different filter topology.

In [10], time-varying coefficients are used to introduce a clipping function in the feedback loop of an IIR filter, in order to reproduce the behaviour of analog voltage controlled filters. In [11] it is shown that this method affects the frequency response of a resonant filter by increasing its bandwidth and moving its centre frequency. The use of IIR coefficients varying on a sample-by-sample basis has been exploited previously in [12] where feedback amplitude modulation is used for sound synthesis and in [13] where time-varying fractional delays are used to model non-linear vibrating strings.

In this paper we will present a physically-informed model for an inductor, with its characteristic non-linearity caused by the saturation of the magnetic core [14]. Non-linear differential equations and a state-space model to solve the non-linear transformer are presented in [15], whereas a Wave Digital Filter approach can be found in [16].

From a physical standpoint, the saturation of the core in an inductor affects the present value of its inductance. From this consideration we will build an infinite impulse response (IIR) linear filter whose coefficients are updated at every time step using the actual value of the inductance given by the current saturation state of its core. This will produce a delay-free loop which we will address using a variation on the classic 1-sample delay approach, widely used in the literature ([17, 18]), and linearizing the system around the operating point. D'angelo recently discussed the linearization of a non-linear system around an operating point to solve a transistor ladder filter [19], generalizing the delay-free loops resolution method in [20].

The physics of the non-linear inductor is reviewed in Section 2. Section 3 will present a reference non-linear discrete-time model for the inductor which will be used to evaluate the approximated model presented in Section 4. Results and discussion follow in Section 5 and Section 6 respectively.

2. PHYSICS OF INDUCTORS

An inductor is a passive component with inductive behavior, usually built using a coil of wire winded on a core made of ferromagnetic material, such as ferrite. While inductors are often modeled as linear components, most real inductors exhibit non-linear

behavior caused primarily by the progressive saturation of their ferromagnetic core. The distortion caused by the core occurs primarily for signals with large currents and low frequencies.

We present here a simplified model for the inductor which models the saturation of the core but does not take into account losses, hysteresis and parasitic parameters.
From Faraday's laws we have, for a solenoid:

$$\frac{dB}{dt} = \frac{V_L}{NS} \tag{1}$$

where B is the magnetic flux density in the inductor core, V_L is the voltage across the inductor, S is the area of the section of the core and N is the number of turns in the inductor. Ampere's law gives the magnetizing force H for a solenoid traversed by a current I_L as: [21]

$$H = \frac{NI_L}{l} \tag{2}$$

and l is the length of the induction path. In an ideal inductor there is a linear relation between the flux density and the magnetizing force:

$$B = \mu H \tag{3}$$

where μ is the absolute magnetic permeability of the core, defined as:

$$\mu = \mu_0 \mu_i \tag{4}$$

where μ_0 is the vacuum permeability and $\mu_i \geq 1$ is the relative permeability of the magnetic core. In the case of a ferromagnetic core, however, the magnetic flux density cannot be increased above a certain value. This value is called magnetic flux density saturation and depends on the material and geometry of the core.

For low flux density levels, Eq. (3) is valid and the inductor can be considered as a linear component. As the core approaches the saturation level B_{sat}, the relation between H and B becomes non linear, the magnetic characteristics of the core change from those of a ferromagnetic material to those of a paramagnetic material and the value of μ progressively changes from being $\mu = \mu_i \cdot \mu_0$ when $B = 0$ to being approximately $\mu = \mu_0$ when $B = B_{sat}$. The Fröhlich-Kennelly relation gives the following relation between B and H for a ferromagnetic core: [22]

$$B = \frac{H}{c + b|H|} \tag{5}$$

where b and c are defined as

$$b = \frac{1 - \sqrt{\frac{1}{\mu_i}}}{B_{sat}}$$
$$c = \frac{1}{\mu_0 \mu_i}$$

The B-H relation described by these formulas is shown in Fig. 1. For small values of $|H|$ and/or large values of B_{sat}, Eq. (5) is equivalent to Eq. (3), thus explaining the linear behaviour at low currents.
The inductance L of a solenoid is derived by Ampere's law as: [21]

$$L = \frac{\mu N^2 S}{l} \tag{6}$$

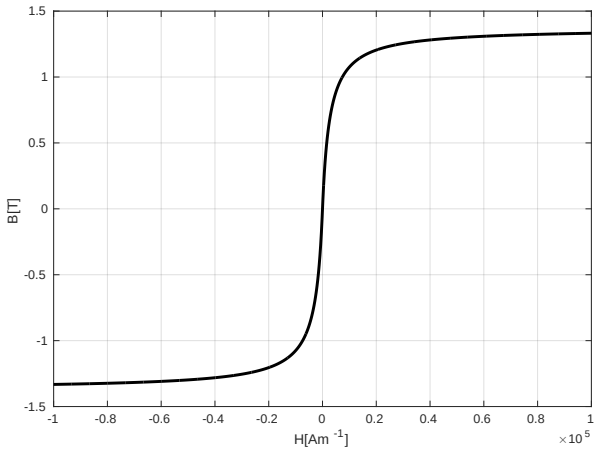

Figure 1: Anhysteretic B-H curve according to the Fröhlich model for an inductor with a ferrite core ($u_i = 400$, $B_{sat} = 1.3$)

where N, S, l, μ are the physical parameters of the inductor described above. As denoted by Eqs. (3) and (5), μ is not constant and its value can drop by several orders of magnitude as the core progressively saturates and this is reflected directly on the value of the inductance through Eq. (6).

3. DISCRETIZATION OF THE NON-LINEAR INDUCTOR

In order to solve a circuit including a non-linear inductor in the discrete-time domain, Eqs. (1), (2) and (5) have to be discretized. This is straightforward for Eqs. (2) and (5):

$$H[n] = \frac{N}{l} I_L[n] \tag{7}$$

$$B[n] = \frac{H[n]}{c + b|H[n]|} \tag{8}$$

while Eq. (1) requires an integration formula. The solution to an equation of the form:

$$\frac{dx}{dt} = f(x,t) \tag{9}$$

is given in the discrete-time domain by the backward Euler formula as: [23]

$$x[n] = x[n-1] + Tf(x[n]) \tag{10}$$

where T is the sampling period of the discrete-time system. This formula, when applied to Eq. (1), yields:

$$B[n] = B[n-1] + \frac{T}{NS} V_L[n] \tag{11}$$

Combining Eqs. (7), (8) and (11), we obtain:

$$V_L[n] = \frac{NS}{T} \left(\frac{\frac{N}{l} I_L[n]}{c + \frac{bN}{l} |I_L[n]|} - B[n-1] \right) \tag{12}$$

Where $V_L[n]$ is the voltage across an inductor at a time instant n given the current through it $I_L[n]$ and the magnetic field at the previous time instant $B[n-1]$.

3.1. High pass filter

We now consider the circuit in Fig. 2. In this circuit low frequencies from the input V_i will find an easier path to ground through the inductor than high frequencies, therefore, considering node V_o as the output, the circuit will act as a high pass filter. For the circuit in Fig. 2, the current through the inductor is:

$$I_L[n] = \frac{V_i[n] - V_o[n]}{R} \tag{13}$$

while the voltage across the inductor is:

$$V_L[n] = V_o[n] \tag{14}$$

Substituting these values in Eqs. (7), (11) and (12) gives:

$$B[n] = B[n-1] + \frac{T}{NS} V_o[n] \tag{15}$$

$$V_o[n] = \frac{NS}{T} \left(\frac{\frac{N}{l} \frac{V_i[n] - V_o[n]}{R}}{c + \frac{bN}{l} \left| \frac{V_i[n] - V_o[n]}{R} \right|} - B[n-1] \right) \tag{16}$$

Combining Eqs. (15) and (16) we obtain the following system equation for the discretized version of the circut in Fig. 2 with a non-linear inductor.

$$V_o^2[n]\beta[n] - V_o[n]\gamma[n] - \delta[n] = 0 \tag{17}$$

with

$$\beta[n] = bNTk[n]$$
$$\gamma[n] = clRT + bNTk[n]V_i[n] + N^2S - bN^2Sk[n]B[n-1]$$
$$\delta[n] = clNRSB[n-1] - bN^2Sk[n]B[n-1]V_i[n] + N^2SV_i[n]$$

in which, k is the sign of the current through the inductor at time instant n, $V_i[n]$ is the voltage input to the system and $B[n-1]$ is computed at each time step using Eq. (15). Eq. (17) is – strictly speaking – a non-polynomial equation as it contains $k = sign(V_o - V_i)$ and should then be solved using iterative numerical approaches (e.g. Newton Method). On the other hand, it can be considered as two distinct second-order polynomials – one with $k = 1$ and one with $k = -1$. Solving these two polynomials will produce four solutions for V_o, of which one and only one will be real and therefore acceptable.

The following schedule can thus be used to find the output $V_o[n]$ of the system for every n:

1. Solve Eq. (17) as explained above to obtain $V_o[n]$. For $n = 0$ assume $B[n-1] = 0$
2. Compute $B[n]$ using Eq. (15)

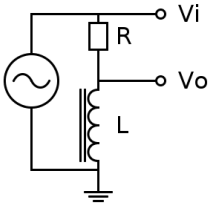

Figure 2: Passive high pass filter

3.2. Low pass filter

We now consider the circuit in Fig. 3. In this circuit high frequencies from the input V_i will be attenuated while passing through the inductor more than low frequencies, therefore, considering node V_o as the output, the circuit will act as a low pass filter. In this case the current through and the voltage across the inductor are, respectively:

$$I_L[n] = \frac{V_o[n]}{R} \tag{18}$$

$$V_L[n] = V_i[n] - V_o[n] \tag{19}$$

Substituting these values in Eqs. (7) and (11) and going through passages similar to those described in Section 3.1 we obtain:

$$V_o^2[n]\epsilon[n] + V_o[n]\zeta[n] + \eta[n] = 0 \tag{20}$$

with

$$\epsilon[n] = bNTk[n]$$
$$\zeta[n] = bN^2Sk[n]B[n-1] - clRT + bNTk[n]V_i[n] - N^2S$$
$$\eta[n] = clNRSB[n-1] + clRTV_i[n]$$

where $k[n] = sign(V_o[n])$ and for which the same considerations made above for the resolution of Eq. (17) are valid.

4. APPROXIMATION OF THE NON-LINEAR INDUCTOR WITH A VARIABLE INDUCTANCE

The reference model presented in Section 3 solves the non-linear electronic circuits proposed using non-linear equations. A different approach is presented in this section which solves the same circuits using time-varying linear filters informed by the physical behaviour of the non-linearity under exam.

In Section 2 we showed that the change in the permeability of the core of an inductor as it approaches saturation affects the effective inductance of the core. The non-linear behaviour is modeled here using a time-varying value for the inductance which is, for each time instant, determined by the current value of the core permeability.

The incremental magnetic permeability of a ferromagnetic material is the rate of change of magnetic flux density with respect to the magnetizing force and is given, in its differential definition, by: [24]

$$\mu_{inc} = \frac{dB}{dH} \tag{21}$$

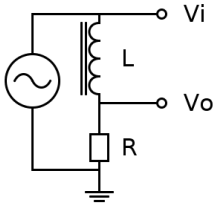

Figure 3: Passive low pass filter

For a real inductor, according to the Fröhlich model, μ_{inc} is given combining this with Eq. (5):

$$\mu_{inc} = \frac{dB}{dH} = \frac{c}{(c + b|H|)^2} \tag{22}$$

Remembering Eqs. (7) and (22), the time-discrete formulation for μ_{inc} is:

$$\mu_{inc}[n] = \frac{c}{(c + \frac{bN}{l}|I_L[n]|)^2} \tag{23}$$

The equation of the inductance of a solenoid as given by Eq. (6) is discretized as:

$$L[n] = \frac{\mu_{inc}[n] N^2 S}{l} \tag{24}$$

Which, combined with Eq. (23), gives:

$$L[n] = \frac{cN^2 S}{l(c + \frac{bN}{l}|I_L[n])^2} \tag{25}$$

4.1. High pass filter

If we consider the inductor in Fig. 2 to be ideal, the cutoff frequency F_c of the filter can be computed from the values of its electronic components as:

$$F_c = \frac{R}{2\pi L} \tag{26}$$

We can discretize the circuit under exam using the well-known bilinear transform. If the component values were time-invariant, the z-transform of the first-order highpass filter would be:

$$H(z) = \frac{2L - 2Lz^{-1}}{RT + 2L + z^{-1}(RT - 2L)} \tag{27}$$

If we now consider the inductor to have a saturating core, the value of L actually changes at every sample, according to Eq. (25). Comparing Eqs. (25) and (26) it emerges that as the current through the inductor increases, the actual inductance value is decreased and consequently the cutoff frequency increases.

As a consequence, the filter coefficients in Eq. (27) will also change over time. Considering the time-varying elements, the finite difference equation for this system is, therefore:

$$V_o[n] = b_0[n]V_i[n] + b_1[n]V_i[n-1] - a_1[n]V_o[n-1] \tag{28}$$

where:

$$\begin{aligned} b_0[n] &= 2L[n]/(RT + 2L[n]), \\ b_1[n] &= -2L[n]/(RT + 2L[n]), \\ a_1[n] &= (RT - 2L[n])/(RT + 2L[n]) \end{aligned} \tag{29}$$

For the circuit in Fig. 2, $L[n]$ depends on the instantaneous current through the inductor, as given by Eq. (13), which, in turn, depends on $V_o[n]$. Therefore $L[n]$ cannot be computed before $V_o[n]$ and it cannot appear in the right hand side of Eq. (28). This constraint leads to an uncomputable loop, also known as delay-free loop [25]. To eliminate the delay free loop we must use an approximate value for $I_L[n]$ which does not depend on $V_o[n]$.

We can estimate a value $V_o'[n] \approx V_o[n]$ by linearizing the output signal around time instant $n-1$ and estimating the value of $V_o'[n]$ using linear extrapolation. Given the discrete-time differentiation of $V_o[n]$

$$\Delta V_o[n] = V_o[n] - V_o[n-1] \tag{30}$$

we can write

$$V_o'[n] = V_o[n-1] + \Delta V_o[n-1] \tag{31}$$

Given a parameter $\alpha \in [0, 1]$, we can define an estimated value $V_o'(n, \alpha)$ for the output voltage at every time instant between $n-1$ and n by linearly interpolating between $V_o[n-1]$ and $V_o'[n]$ as:

$$V_o'(n, \alpha) = \alpha \cdot V_o[n-1] + (1 - \alpha) \cdot V_o'[n] \tag{32}$$

which, for $\alpha = 1$ equals $V_o[n-1]$ and for $\alpha = 0$ equals $V_o'[n]$. In order to appropriately compute the current through the inductor, the input and output voltage must be considered at the same instant in time, therefore we also define $V_i'(n, \alpha)$ as the linear interpolation between $V_i[n-1]$ and $V_i[n]$, parametrized by α:

$$V_i'(n, \alpha) = \alpha \cdot V_i[n-1] + (1 - \alpha) \cdot V_i[n] \tag{33}$$

Now we can compute approximate value for $I_L[n]$ parametrized by α by replacing V_o with $V_o'(n, \alpha)$ and V_i with $V_i'(n, \alpha)$ in Eq. (13):

$$I_{L_\alpha}[n] = \frac{V_i'(n, \alpha) - V_o'(n, \alpha)}{R} \tag{34}$$

4.2. Low pass filter

The z-transform of the low pass filter in Fig. 3:

$$H(z) = \frac{RT + RTz^{-1}}{RT + 2L + z^{-1}(RT - 2L)} \tag{35}$$

We can derive the equations for the filter coefficients similarly to what has been done in the previous paragraph. In the case of a real inductor, the value of $L[n]$ is, again, time-varying and it depends on the current through the inductor $I_L[n]$ for each instant n.

As such current is not known in advance, we need to use an approximate value for $I_L[n]$ when computing the filter coefficients. Analogously to what has been done for the high pass filter in Section 4.1, using the same formulas for linear extrapolation as in Eq. (31) and linear interpolation as in Eq. (32) to obtain $V_o'(n, \alpha)$, we can write the estimated current through the inductor, parametrized by α, by replacing V_o with $V_o'(n, \alpha)$ in Eq. (18):

$$I_{L_\alpha}[n] = \frac{V_o'(n, \alpha)}{R} \tag{36}$$

5. RESULTS

For the evaluation of the approximated saturating inductor model we created a digital model of the high pass circuit in Fig. 2 and solved it using both the model involving non-linear equations described in Section 3, used as a reference, and the approximate model introduced in Section 4. Results for the low pass circuit in Fig. 3 are not explicitly reported here for brevity, but the findings are very similar to those outlined below for the high pass filter.

We performed our tests using the parameter values listed in Table 4 over all of the possible combinations of the following parameters:

Input level [V]	**Input signal** 15Hz	45Hz	89Hz	179Hz	238Hz	953Hz	3810Hz	7620Hz	15240Hz	19050Hz	Noise	Bass	Guitar
1	0.034	0.041	0.041	0.041	0.041	0.041	0.041	0.041	0.041	0.041	0.042	0.041	0.041
10	0.024	0.039	0.041	0.041	0.041	0.041	0.041	0.041	0.041	0.041	0.053	0.046	0.041
50	0.203	0.193	0.026	0.039	0.040	0.041	0.041	0.042	0.042	0.042	0.172	0.115	0.043
100	0.397	0.669	0.572	0.025	0.035	0.041	0.042	0.042	0.042	0.042	0.330	0.256	0.046
200	0.706	1.360	1.750	1.515	0.501	0.041	0.042	0.042	0.043	0.043	0.470	1.130	0.058

Table 1: High-pass filter: frequency-domain RMS error (%) for different signals and input voltages, with $\alpha = 1$ and sampling rate=48kHz

Sampling rate [kHz]	**Input signal** 15Hz	45Hz	89Hz	179Hz	238Hz	953Hz	3810Hz	7620Hz	15240Hz	19050Hz	Noise	Bass	Guitar
12	2.703	4.944	6.032	4.412	0.943	0.165	0.175	-	-	-	3.425	3.740	0.221
24	1.390	2.621	3.295	2.688	0.775	0.082	0.084	0.085	-	-	1.152	2.123	0.114
48	0.706	1.360	1.750	1.515	0.501	0.041	0.042	0.042	0.043	0.043	0.470	1.130	0.058
96	0.356	0.694	0.908	0.811	0.286	0.020	0.021	0.021	0.021	0.021	0.434	0.579	0.030
192	0.179	0.351	0.463	0.421	0.153	0.010	0.010	0.010	0.010	0.010	0.279	0.289	0.015
384	**0.090**	**0.177**	**0.234**	**0.214**	**0.079**	**0.005**	**0.005**	**0.005**	**0.005**	**0.005**	**0.154**	**0.142**	**0.008**

Table 2: High-pass filter: frequency-domain RMS error (%) for different signals and sampling rates with $\alpha = 1$ and input level=200V

α	**Input signal** 15Hz	45Hz	89Hz	179Hz	238Hz	953Hz	3810Hz	7620Hz	15240Hz	19050Hz	Noise	Bass	Guitar
0	1.062	2.072	2.600	2.410	0.904	0.211	1.475	11.821	533.597	533.597	51.414	1.019	0.622
0.25	0.758	1.480	1.891	1.684	0.582	0.153	0.780	5.894	479.974	479.974	45.540	0.620	0.538
0.5	0.538	1.055	1.378	1.135	0.341	0.095	0.250	1.537	336.812	336.812	37.176	**0.485**	0.448
0.75	**0.517**	**1.006**	**1.319**	**1.067**	**0.316**	**0.031**	0.064	0.854	211.559	211.559	20.818	0.742	0.311
1	0.706	1.360	1.750	1.515	0.501	0.041	**0.042**	**0.042**	**0.043**	**0.043**	**0.470**	1.130	**0.058**

Table 3: High-pass filter: frequency-domain RMS error (%) for different signals and values of α with sampling rate=48kHz and input level=200V

1. sampling frequencies:
   12kHz, 24kHz, 48kHz, 96kHz, 192kHz, 384kHz.
2. audio signals:
   (a) Sine waves at frequencies:
   15Hz, 45Hz, 89Hz, 179Hz, 238Hz, 953Hz, 3810Hz, 7620Hz, 15240Hz, 19050Hz, length 10 seconds
   (b) White noise sample, length 10 seconds
   (c) Electric bass guitar sample, length 6.6 seconds
   (d) Electric guitar sample, length 3.1 seconds
3. a set of amplitudes: 1V, 10V, 50V, 100V, 200V
4. a set of values for the linear interpolation parameter α: 0.25, 0.5, 0.75, 1

We skipped tests on sine waves whose frequency was above the Nyquist frequency of the sampling rate. For sampling frequencies of 48kHz and above the result signals have been bandlimited to a maximum frequency of 20kHz before computing error figures. Given a sampling rate, an input signal and an amplitude, the outputs of the approximate model for each different α have been compared to the output of the reference model.

$R[\Omega]$	μ_i	$B_{sat}[T]$	N	$S[cm^2]$	$l[cm]$
100	400	1.3	1000	1	2

Table 4: Physical parameters used in the simulation.

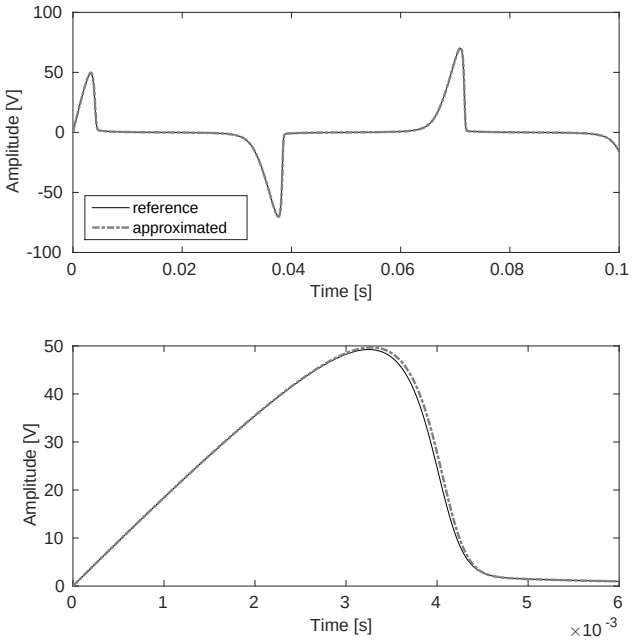

Figure 4: Time domain waveforms for the reference and approximated high pass filter for sampling frequency 48kHz, signal frequency 15Hz, input level 200V, $\alpha = 1$. Large time scale (top) and detail (bottom)

Fig. 4 displays the time domain voltage signal of a 15Hz sinusoid of peak amplitude 200V processed through the high pass filter. The time domain waveforms are very similar. Fig. 4 (bottom) shows that only by zooming in on the time axis we can notice the difference: the drop in voltage caused by the saturation of the core is slightly delayed in the approximated waveform. This can be easily explained considering that in the approximated model the value for the flux density is computed based on the value of the current at the previous time sample, which causes an inherent delay in the response. Fig. 5 shows that the flux density is in fact

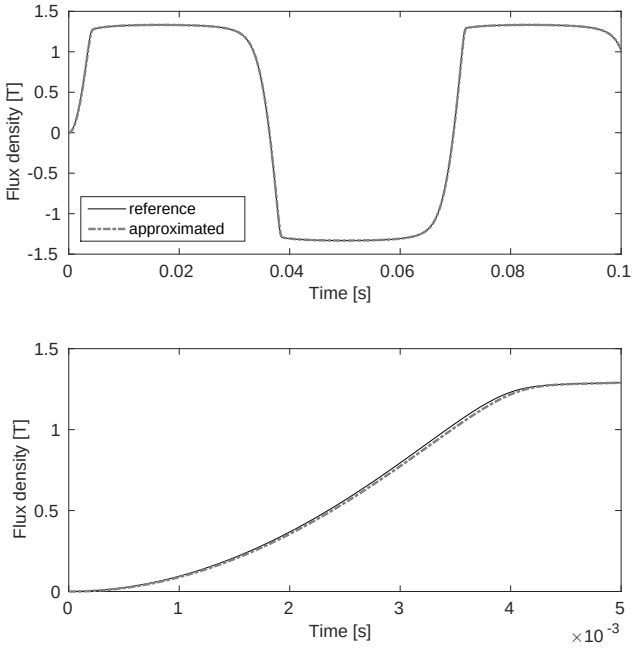

Figure 5: Time domain waveforms of the flux density for the signal in Fig. 4. Large time scale (top) and detail (bottom).

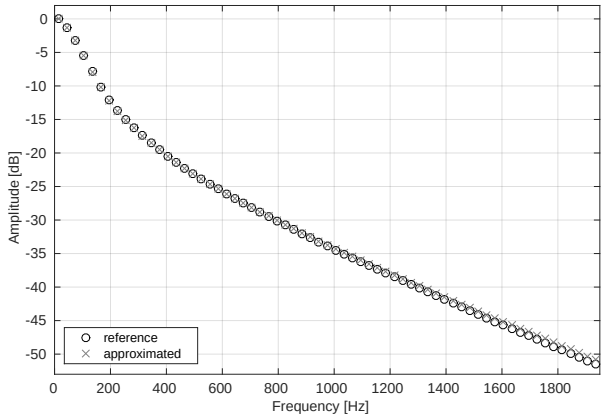

Figure 6: Peaks of the spectrum of the signal in Fig. 4

slightly delayed with respect to the reference.

The RMS error between the two time-domain voltage signals is 2.45%. This rather large error figure is justified by the fact that the discrepancy between the two waveforms occurs around a rapid voltage drop. As human perception of an audio signal is linked more closely to its frequency content than to its time-domain representation, we find it more relevant to reference the THD, THD+N and frequency domain RMS error figures for the purposes of this evaluation.

Fig. 6 displays the reference and approximated signal in the frequency domain. They are very similar, with a total RMS error in the frequency domain as small as 0.71%. While the match is almost perfect for the lower harmonics, a small discrepancy arises

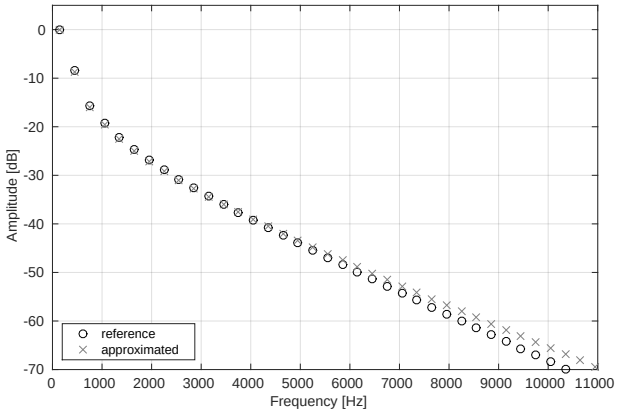

Figure 7: Peaks of the spectrum of a 150Hz sinusoid processed through the high pass filter circuit, sampled at 48kHz

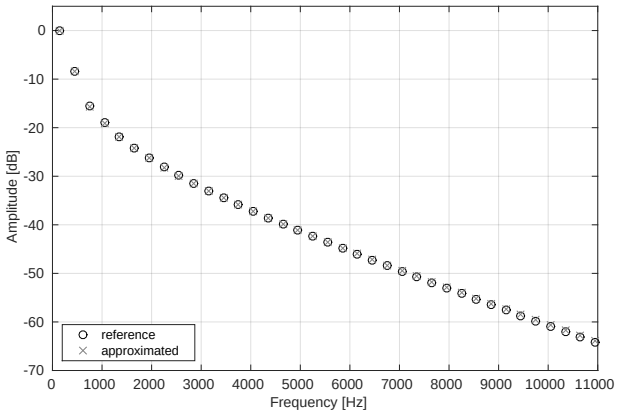

Figure 8: Peaks of the spectrum of a 150Hz sinusoid processed through the high pass filter circuit, sampled at 384kHz

from the 90th harmonic (1350Hz and above). No noise or spurious frequencies have been introduced by the approximated model, as denoted by the fact that the THD and the THD+N values are exactly the same.

Performing the same analysis on a 150Hz signal gives a time-domain RMS error of 8.63% and a frequency-domain RMS error of 1.69%. The spectrum of the signal is shown in Fig. 7. The discrepancies in the spectral amplitudes begin to arise from about 4950Hz (33rd harmonic). Again, no spurious frequencies or noise are added.

By increasing the sampling frequency to 384kHz (8 times oversampling), for the 150Hz sinewave we obtain that the time-domain RMS error is cut down to 1.1% and the frequency-domain RMS error is 0.24%. The increase in the sampling rate reduced the effect of the unit delay used in the approximation. The frequency response of this oversampled signal is displayed in Fig. 8. At every time step the value of the inductance $L[n]$ changes according to an estimated value of the current through the inductor, as explained in Section 4.1. Tables 1 to 3 show the frequency domain error figures for each of the test signals. Table 1 shows that the increase in the amplitude of the input signal causes larger errors. This is expected as to a larger amplitude corresponds a faster saturation

of the core and therefore a larger distortion of the output, with a steeper voltage drop in the time domain. Table 2 shows that results are greatly improved by increasing the sampling frequency. The error reduction is proportional to $1/F_s$.

The α parameter, as given by Eq. (34), determines the balance between the weight given to the value $I[n-1]$ of the current measured at the previous time step and the estimated value $I'[n]$ of the current through the inductor at the current time instant, when computing the value $L[n]$ of the inductance at the current time instant. When $\alpha = 0.5$ the estimated value used for the current through the inductor is the average value of the current over the time interval between $n-1$ and n and this is, in theory, the best choice to be used in the computation of $L[n]$, as long as the estimated value $I'[n]$ is reasonably close to the actual value $I[n]$.

Test results in Table 3 show that most of the times $\alpha = 0.75$ performs better than $\alpha = 0.5$ and also that both these values perform poorly when the signal contains significant amounts of energy at higher frequencies. This can be explained by the fact that as the frequency of the signal increases, the linear extrapolation becomes less accurate and $\alpha = 0.75$ performs better than $\alpha = 0.5$ because the overshoot caused by the estimate is mitigated by giving less weight to it. The value of $\alpha = 1$, corresponding to no linear extrapolation being used, was found to be the one that gives best results for a signal of arbitrary frequency content. This effectively corresponds to the introduction of a 1-sample delay so that the filter coefficients are entirely based on the system state at the previous sample instant.

6. DISCUSSION

In this paper we introduced a way to solve a high pass filter circuit containing a non-linear inductor using a time-varying IIR filter, whose block diagram is shown in Fig. 9. The model is physically informed and exploits the fact that the actual inductance value for a solenoid changes according to the saturation of its core. As pointed out in 4.1, these changes affect the frequency response of the filter by modulating its cutoff frequency.

6.1. Performance

The time-variant IIR filters used here to emulate the behavior of a non-linear inductor produced results comparable to the reference model and they did not exhibit any inherent instability. The time domain error due to the intrinsic delay in the approximation does not affect negatively the perceived sound, as it produces rather small error figures in the frequency-domain. For certain combinations of parametes (e.g. large μ_i, large input voltage) ringing and overshoot effects have been observed, due to the sudden change in the filter coefficients. These effects can be attenuated by hard limiting the slew rate of the filter coefficients, imposing a maximum-change-per-sample limit, or otherwise suppressing the transient using one of the techniques proposed in [8].

The use of linear extrapolation to compute an estimate of the inductance value at the current time sample did not improve the results. On the other hand, the model produces good results when not using linear extrapolation, with frequency-domain errors below 1.75% in all the cases under exam and below 1.2% when tested with real-world audio signals.

Inductors mostly saturate at low frequencies, therefore the use of oversampling is not a requirement when modeling this type of non-linearity, as the higher partials generated by the distortion are

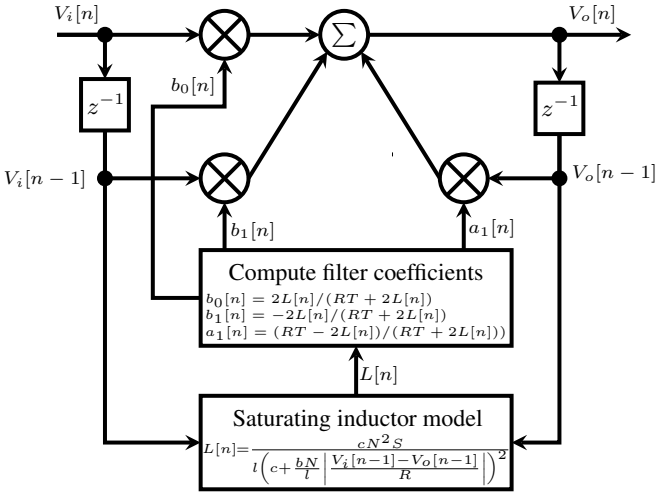

Figure 9: Block diagram of the digital filter for the circuit in Fig. 2, when $\alpha = 1$.

likely to be below the Nyquist frequency even for a sampling rate of 48kHz. Despite this general consideration, the choice of the oversampling factor has to be evaluated on a case-by-case basis, according to the characteristics of the inductor (e.g. saturation flux density), of the circuit (e.g. presence of other non linear elements and filters) and of the expected frequency content of the input signal. Nevertheless, the accuracy of the model takes advantage of oversampling, which reduces the effects of the 1-sample delay and gives better results overall.

As outlined above, Eq. (17) is a particular case which can be solved with lower computational cost than most non-linear equations found in DSP systems. This considered, solving the high pass circuit using the non-linear model and Eq. (17) requires 13 multiplies, 12 additions and 2 square roots per sample. Solving the same circuit with the time-variant IIR filter in Section 4 requires 5 multiplies, 4 additions and 2 divisions per sample. As on modern CPUs the execution time of square roots is greater or equal than the one for divisions, the time-variant IIR model turns out to have a lower computational cost than the non-linear one. Improvements in speed can become even greater when a similar approach is used to model non-linearities which are otherwise solved through computationally-expensive transcendental functions.

The stability and performance of time-variant IIR models have to be evaluated on a case-by-case basis. For instance, modeling of a diode clipper circuit as a time-variant resistor has been attempted by the authors which led to a conditionally-working model that requires oversampling and other adjustments to prevent DC drift of the output.

6.2. Applications

The idea that is at the base of this research, that is the use of time-variant linear filters with recursive coefficient computation to implement non-linearities, proved to be not only achievable, but also well suited for the emulation of a real electronic component, the inductor. This model has been successfully used to extend existing systems, without requiring major re-designs. For instance, it was used to add the non-linearities of the inductor to the wah-wah

pedal model based on the DK-method presented in [26] by simply replacing the static inductance in the circuit with a time-varying one. What emerged from the simulation of the wah-wah pedal is that the current through the inductor was too small to cause audible saturation, when using for the inductor parameters similar to the ones of a real wah-wah inductor. By introducing fictitious physical parameters for the inductor, we allowed the input signal to drive it into saturation. As a result we obtained increased harmonic distortion and a shift of the cutoff frequency of the filter.

The inductor model presented is not complete yet, as a full model of the inductor would require at least to add the hysteresis of the magnetic core. From what we have seen so far, it is reasonable to think that this additional step will not add much to the complexity of the model.

7. REFERENCES

[1] J. Macak, J. Schimmel, and V. Välimäki, "Real-time guitar preamp simulation using modified blockwise method and approximations," *EURASIP Journal on Advances in Signal Processing*, vol. 2011, pp. 20, 2011.

[2] D. T. M. Yeh, "Automated physical modeling of nonlinear audio circuits for real-time audio effects;part II: BJT and vacuum tube examples," *Audio, Speech, and Language Processing, IEEE Transactions on*, vol. 20, no. 4, pp. 1207–1216, May 2012.

[3] K. Meerkötter and R. Scholz, "Digital simulation of nonlinear circuits by wave digital filter principles," in *Circuits and Systems, 1989., IEEE International Symposium on*. IEEE, 1989, pp. 720–723.

[4] S. Petrausch and R. Rabenstein, "Wave digital filters with multiple nonlinearities," in *Signal Processing Conference, 2004 12th European*, Sept 2004, pp. 77–80.

[5] J. O. Smith, *Introduction to Digital Filters with Audio Applications*, W3K Publishing, http://www.w3k.org/books/, 2007.

[6] G. Stoyanov and M. Kawamata, "Variable digital filters," *J. Signal Processing*, vol. 1, no. 4, pp. 275–289, 1997.

[7] J. Laroche, "On the stability of time-varying recursive filters," *Journal of the Audio Engineering Society*, vol. 55, no. 6, pp. 460–471, 2007.

[8] V. Välimäki and T.I. Laakso, "Suppression of transients in time-varying recursive filters for audio signals," in *Proceedings of the 1998 IEEE International Conference on Acoustics, Speech and Signal Processing, 1998*, May 1998, vol. 6, pp. 3569–3572 vol.6.

[9] A. Wishnick, "Time-varying filters for musical applications," in *Proceedings of the 17th International Conference on Digital Audio Effects (DAFx-14)*, 2014, pp. 69–76.

[10] D Rossum, "Making digital filters sound "analog"," pp. 30–33, 1992.

[11] V. Välimäki, S. Bilbao, J. O. Smith, J. S. Abel, J. Pakarinen, and D. Berners, "Virtual analog effects," *DAFX: Digital Audio Effects, Second Edition*, pp. 473–475, 2011.

[12] J. Kleimola, V. Lazzarini, V. Valimaki, and J. Timoney, "Feedback amplitude modulation synthesis," *EURASIP Journal on Advances in Signal Processing*, , no. 434378, 2011.

[13] J. Pakarinen, V. Välimäki, and M. Karjalainen, "Physics-based methods for modeling nonlinear vibrating strings," *Acta Acustica united with Acustica*, vol. 91, no. 2, pp. 312–325, 2005.

[14] D. C. Jiles, J. B. Thoelke, and M. K. Devine, "Numerical determination of hysteresis parameters for the modeling of magnetic properties using the theory of ferromagnetic hysteresis," *Magnetics, IEEE Transactions on*, vol. 28, no. 1, pp. 27–35, 1992.

[15] J. Macak, "Nonlinear audio transformer simulation using approximation of differential equations," *Elektrorevue*, vol. 2, no. 4, December 2011.

[16] R. C. D. de Paiva, J. Pakarinen, V. Välimäki, and M. Tikander, "Real-time audio transformer emulation for virtual tube amplifiers," *EURASIP Journal on Advances in Signal Processing*, vol. 2011, no. 1, pp. 347645, 2011.

[17] T. Stilson and J. Smith, "Analyzing the moog vcf with considerations for digital implementation," in *Proceedings of the 1996 International Computer Music Conference, Hong Kong, Computer Music Association*, 1996.

[18] A. Huovilainen, "Nonlinear digital implementation of the moog ladder filter," in *Proc. Int. Conf. on Digital Audio Effects (Naples, Italy, October 2004)*, 2004, pp. 61–4.

[19] S. D'Angelo and V. Välimäki, "Generalized moog ladder filter: Part ii–explicit nonlinear model through a novel delay-free loop implementation method," *Audio, Speech, and Language Processing, IEEE/ACM Transactions on*, vol. 22, no. 12, pp. 1873–1883, 2014.

[20] A. Härmä, "Implementation of recursive filters having delay free loops," in *Acoustics, Speech and Signal Processing, 1998. Proceedings of the 1998 IEEE International Conference on*. IEEE, 1998, vol. 3, pp. 1261–1264.

[21] D. J. Griffiths, *Introduction to electrodynamics*, vol. 3, Prentice hall Upper Saddle River, NJ, 1999.

[22] D. C. Jiles, *Introduction to Magnetism and Magnetic Materials, Second Edition*, Taylor & Francis, 1998.

[23] D. T. M. Yeh, *Digital implementation of musical distortion circuits by analysis and simulation*, Ph.D. thesis, Stanford University, 2009.

[24] "Incremental magnetic permeability," in *Computer Science and Communications Dictionary*, pp. 763–763. Springer US, 2001.

[25] G. Borin, G. De Poli, and D. Rocchesso, "Elimination of delay-free loops in discrete-time models of nonlinear acoustic systems," *Speech and Audio Processing, IEEE Transactions on*, vol. 8, no. 5, pp. 597–605, 2000.

[26] M. Holters and U. Zölzer, "Physical modelling of a wah-wah effect pedal as a case study for application of the nodal DK method to circuits with variable parts," in *Proceedings of the 14th International Conference on Digital Audio Effects DAFx11*, 2011, pp. 19–23.